

We are IntechOpen, the world's leading publisher of Open Access books Built by scientists, for scientists

4,800

Open access books available

122,000

International authors and editors

135M

Downloads

Our authors are among the

154

Countries delivered to

TOP 1%

most cited scientists

12.2%

Contributors from top 500 universities



WEB OF SCIENCE™

Selection of our books indexed in the Book Citation Index
in Web of Science™ Core Collection (BKCI)

Interested in publishing with us?
Contact book.department@intechopen.com

Numbers displayed above are based on latest data collected.
For more information visit www.intechopen.com



Impact of Surface Topography of Tools and Materials in Micro-Sheet Metal Forming

Tetsuhide Shimizu, Ming Yang and Ken-ichi Manabe

Additional information is available at the end of the chapter

<http://dx.doi.org/10.5772/48296>

1. Introduction

Microforming technology has been receiving much attention as one of the most economical mass production methods for micro components (Geiger et al., 2001). Especially, metal foils have the great advantage to produce high-aspect three-dimensional shapes by miniaturizing the process dimensions of sheet metal forming technologies.

Since the relative ratio of the surface area to the volume of metal foils becomes significantly larger with miniaturization, tribological behaviour is of great significance for the micro-sheet formability. Over the last decade, basic researches of the size effect of tribology in microforming have been performed worldwide (Vollertsen et al., 2009). One of the representative reports of scale effect in bulk metal forming is the double-cup-extrusion (DCE) test (Engel, 2006). By scaling the diameter of CuZn15 specimen from 4mm to 0.5mm, the scaled DCE test was conducted. Identified with a FE analysis, the significant increase of the friction factor m with decreasing the scale was confirmed. Another reports regard to the size effect of coefficient of friction in bulk metal forming was done by Putten et al. (Putten et al., 2007). The scaled plane strain compression tests were conducted with the aim of application on flat rolling. As similar tendency as DCE test, the friction coefficient increased with decreasing scale dimension.

The work focused on the sheet metal forming has been done by Vollertsen and Hu (Vollertsen & Hu, 2006, 2007). The strip drawing method allowing the determination of friction parameters for micro-deep drawing was developed. It was shown that the friction coefficient again increased with decreasing the size. Additionally, the scale dependent friction coefficient was determined by strip drawing test and the calculated value was introduced to the FEM simulation. Especially if the non-uniform pressure distribution was

taken into account in the deep drawing simulation, relative good results were derived for different dimensions (Vollertsen et al., 2008).

These tendencies of the increasing friction coefficient with decreasing dimension in many experiment of forming process have been mainly explained by the “lubricant pocket model” (Engel, 2006). The lubricant pocket model is the only one available model for the description of size effects in lubricated friction (Vollertsen et al., 2009). The basic feature of describing the size effect based on this model is that the increasing relative ratio of OLPs (Open lubricant pockets), which cannot keep the lubricant. With decreasing the scale dimension, the relative ratio of OLPs increases and it results in the increase of friction resistance (Engel, 2006). As overviewed above, the overall investigation suggests the low effect of lubricant in micro-scale region.

From the other point of view of:

1. Dirt handling of the tiny work pieces,
2. Contamination of fine products,
3. Lubricant clogging between the micro scale clearance, and
4. Unstable formability due to the high sensitivity of the variation of lubricant quantity or the effects of meniscus and viscous forces,

the microforming process would be preferred not to use a lubricant (Aizawa et al., 2010).

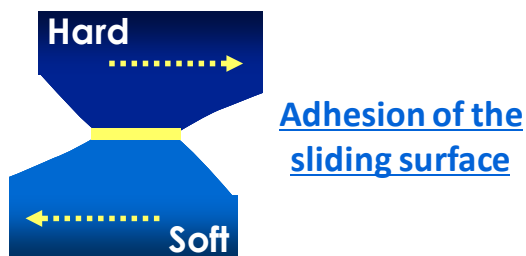
In response to these findings, the activity of the application of the coating treatment on the die substrate, targeting the microforming, is gradually increasing. Hanada et al. fabricated a micro-die utilizing chemical vapour deposition (CVD) diamond coating (Hanada et al., 2003). The surface roughness of the diamond dies was approximately 10 nm, and the diamond dies showed good lubricating ability in the microcoining of polymethylmethacrylate (PMMA). Fuentes et al. investigated the tribological properties of Al thin foils (0.2mm nominal thickness) in sliding contact with PVD-coated carbide forming-tools for microforming (Fuentes et al., 2006). Uncoated, CrN-coated and WC-C-coated tools were tested, using a pin-on-disk configuration. They have shown that the sticking of Al was retarded using low friction magnetron sputtered WC-C-coated carbides. Fujimoto et al. proposed a novel surface treatment process for micro-dies (Fujimoto et al., 2006). They developed a high-energy ion beam irradiation for finishing die-surfaces and a CVD diamond-like carbon (DLC) was coated on the die surface after finished. They have succeeded to reduce the surface roughness by ion beam irradiation process and the high wear resistance of the DLC coating was demonstrated with the 50,000 shots of the microbending tests. In the recent work on the coating treatment for micro die, an impressive coating technology was proposed by Aizawa et al. (Aizawa et al., 2010). The nano-laminated DLC coating was invented and applied to improve the coated tool life, where delamination of coated layers was significantly retarded or saved by optimum interlayer and nano-scopic lamination of DLC sublayers. Micro stamping system, which included the severe wearing condition of ironing and bending step, was employed in the 10,000 shots progressive dry micro-stamping, where SKD-11 punches underwent severe wear in stamping of AISI-304 stainless sheets or pure titanium sheets.

Although these applied researches on the field of dry-microforming are well developed for the practical application, the basic research on the dry friction behaviour during microforming was quite few and it was only worked for bulk metal forming (Vollertsen et al., 2009). Krishnan et al. investigated the scale effect on dry friction by scaled forward extrusion test of brass (Cu:Zn 70:30) with the scale range of 0.57-1.33mm in outer diameter of extruded pin (Mori et al., 2007; Krishnan et al., 2007). In addition, the other author conducted the scaled ring compression test of CuZn15 alloy with different grain size. The test was scaled in the range of 0.5 to 4.25mm of ring inner diameter (Vollertsen et al., 2009). Although the purpose of those studies is to determine the size effect under dry friction, the statement for the size effect of dry friction seems to be very doubtful and there are no general explanations.

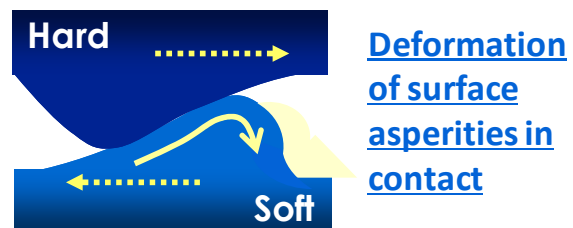
According to the tribology theory for dry contact friction (Bhushan, 2003), friction resistance is contributed by:

- Adhesion of the sliding surface,
- Deformation of surface asperities in contact,
- Plowing by wear particles and hard asperities, and
- So called, ratchet mechanism, which is due to a lateral force required for the contact asperities to climb against each other.

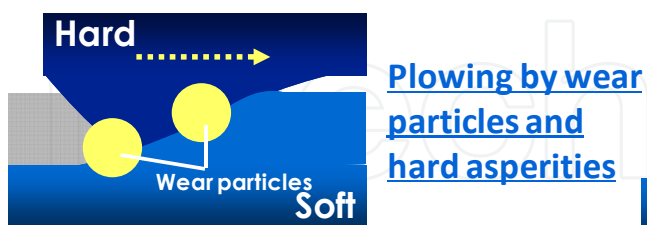
■ μ_a : Adhesion component



■ μ_d : Deformation component



■ μ_p : Plowing component



■ μ_r : Ratchet component

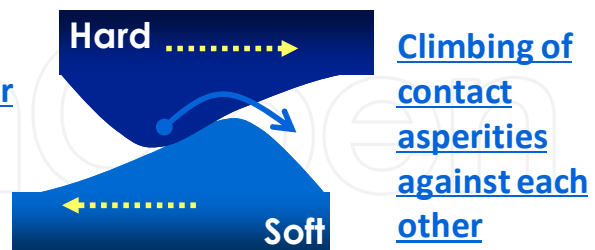


Figure 1. Contributions of the four different components of friction coefficient under dry friction

As illustrated in Fig.1, the geometry of surface asperities would contribute to the real area of contact and sliding resistance, and it is a dominant factor over the dry friction behaviour.

However, basic research on the meso-scale tribological behaviour of dry friction, such as the contact interaction of the surface asperities, is not well discussed, especially for micro-sheet metal forming (Vollertsen et al. 2009). In view of the surface functionalization and the structural optimisation, construction of the surface design guide based on the

characterization of tribological behaviour under dry friction is a pressing need for the further high precision forming process design.

In view of the significant importance of tribology in micro-sheet metal forming, this chapter creates an overview of the effect of surface topography of tools and workpieces on micro-sheet formability. Starting with an introduction of the newly developed micro-deep drawing experimental system and that of a finite element simulation model with surface asperities, the impact of surface topography on the tiny micro-scale forming behaviour is discussed.

2. Development of micro-deep drawing experimental system

The experimental system for micro-deep drawing is newly developed with a goal for highly accurate forming operation with a good reproducibility in experimental results. The system consists of (a) micro-drawing die assembly, (b) desktop size miniature press machine, (c) control panel and (d) compact feeding device. Fig. 2 shows the appearance of developed micro-deep drawing experimental system.

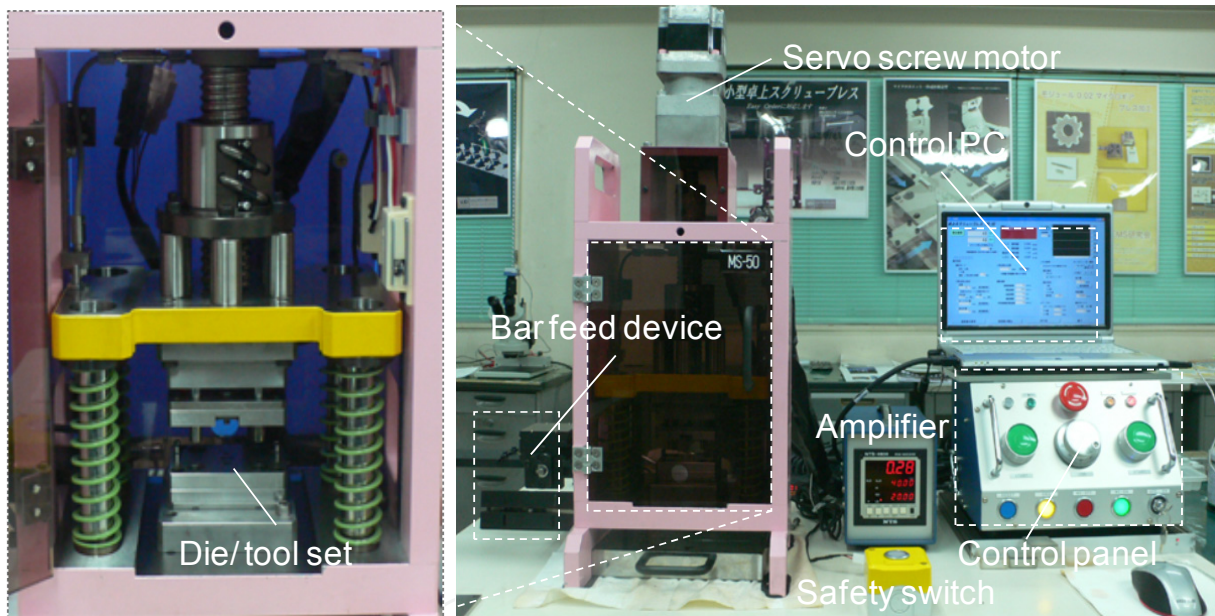


Figure 2. Appearance of micro deep drawing experimental system

2.1. System specification and design of die assembly

Developed micro-drawing die assembly is devised to improve the handling characteristics of tiny blank and to enhance the positioning accuracy of central axis of drawing process. A blanking-drawing process, which combines the blanking and drawing, is adopted and tool set is designed. The schematic illustration of micro-blanking-drawing process is shown in Fig.3. The tool of drawing die combined with the blanking punch is able to form directly from the blanking material to drawing micro-cup. In addition, blank holder force during the process is not applied for better reproducibility of the experiment. Instead of the blank holder, the constant gap between the drawing die and the blank holder is designed.

Fig.4 shows the appearance of designed micro-deep drawing die assembly. The die assembly is designed to compact palm-size with around 10cm square. Blanking punch-drawing die is mounted on the upper die, while the blanking die and the drawing punch is set up to the lower die. Furthermore, in order to measure the forming load during the process, the micro-compression load cell (TC-SR50N, TEAC Co.), which has the rating capacity of 50N, is aligned directly below the drawing punch of the lower die.

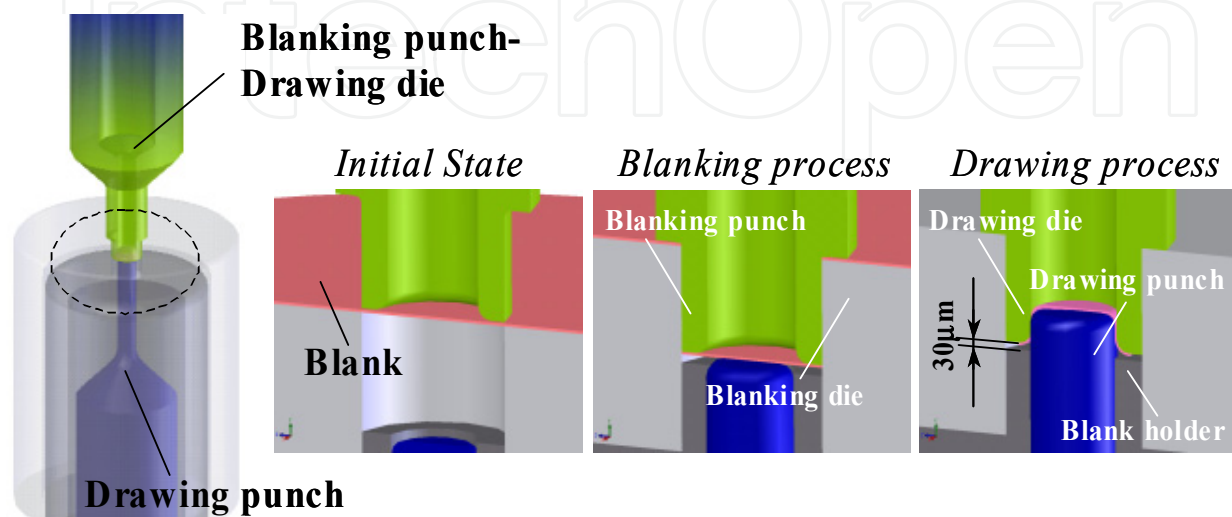


Figure 3. Schematic illustration of micro sequential blanking-drawing process

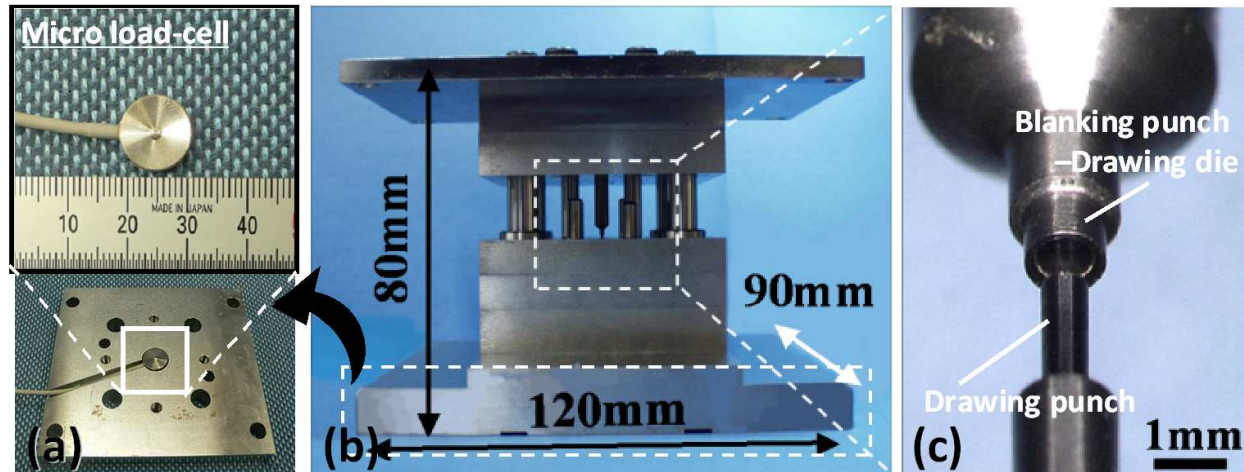


Figure 4. Appearance of designed micro drawing die assembly (a) micro compression load-cell, (b) micro drawing die assembly, (c) tool set of micro sequential blanking-drawing process

The micro-drawing die assembly is mounted on the desktop size miniature press machine (MS-50M, Seki Co.), which is custom-designed for the micro deep drawing experiment by Seki Corporation. The press machine is driven with a servomotor, which has a high motion resolution of 400nm and a maximum instantaneous velocity of 28mm/s. The motion control is based on the high precision digital displacement sensor (GT2 Keyence Co.) mounted on the press machine. In addition, a variety of press ram motion can be realized by developed

controlling program, such as linear or S-curve acceleration and deceleration, inching motion at bottom dead point and motion stop at several displacement for input time length.

Moreover, the compact feeding device is newly developed for the miniature press machine. By using this device, the coiled material of metal foils can be progressively supplied during the process and the continuous transition of the forming behaviour, such as wear of tools, would be able to track in the experiment.

2.2. Fabrication of micro circular cup

By using the developed micro-deep drawing experimental system, a trial test for fabricating the micro-circular cup is carried out. As a first target of the process dimensions for the micro-deep drawing experiment, we aimed to produce the microcups with outer diameter of $500\mu\text{m}$ from the blank of 1.1 mm in diameter and of $20\mu\text{m}$ in thickness. Material used is stainless steel (JIS: SUS304-H), phosphor bronze (JIS: C5191-H), and pure titanium (JIS: TR270C-H) ultra-thin metal foils. Redrawing process is adopted to produce a cup of $700\mu\text{m}$ diameter at the first-stage and $500\mu\text{m}$ diameter at the second-stage. All microtools are made of sintered WC-Co hard alloy (JIS: V20 tungsten-carbide-cobalt alloy), machined by EDM (Electrical discharged machining) and mechanically fined polishing. By adjusting the clearance between die and punch, die corner radius and punch corner radius, the tool dimensions are determined as shown in Fig. 5.

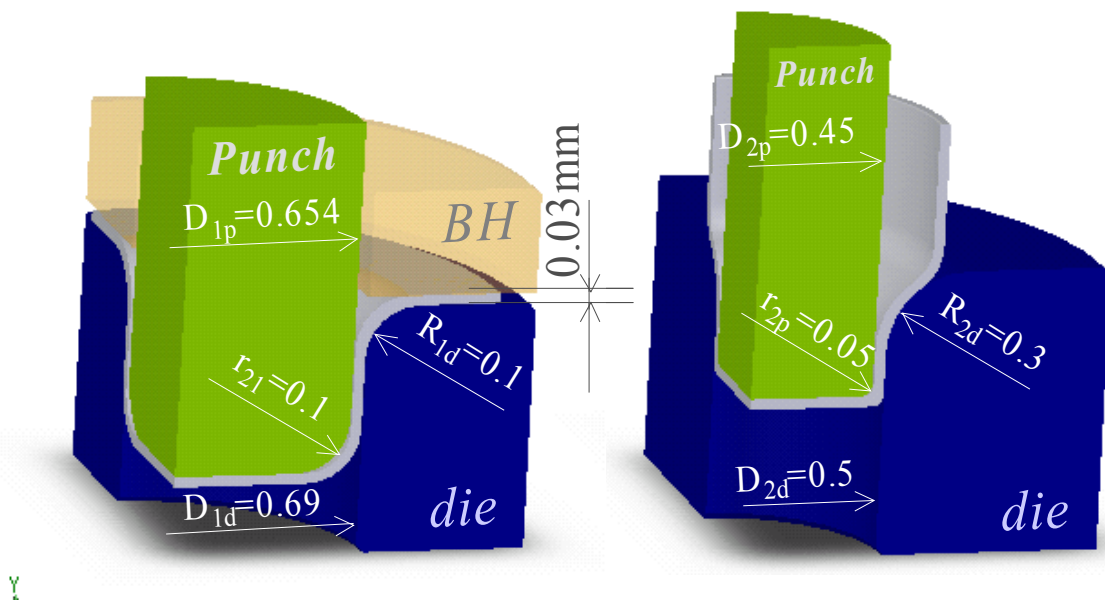


Figure 5. Schematic illustration of tool dimensions for micro-drawing experiment

Fig.6 shows the fabricated microcups on a forefinger and the SEM images of the first-stage and second-stage drawn microcups. The tiny microcups are fabricated successfully by the microforming technology. The micro-deep drawing process is realized by a high-precision blanking-drawing technique, and more than 100 microcups are produced with good reproducibility for every three kinds of materials, as shown in Fig. 7.

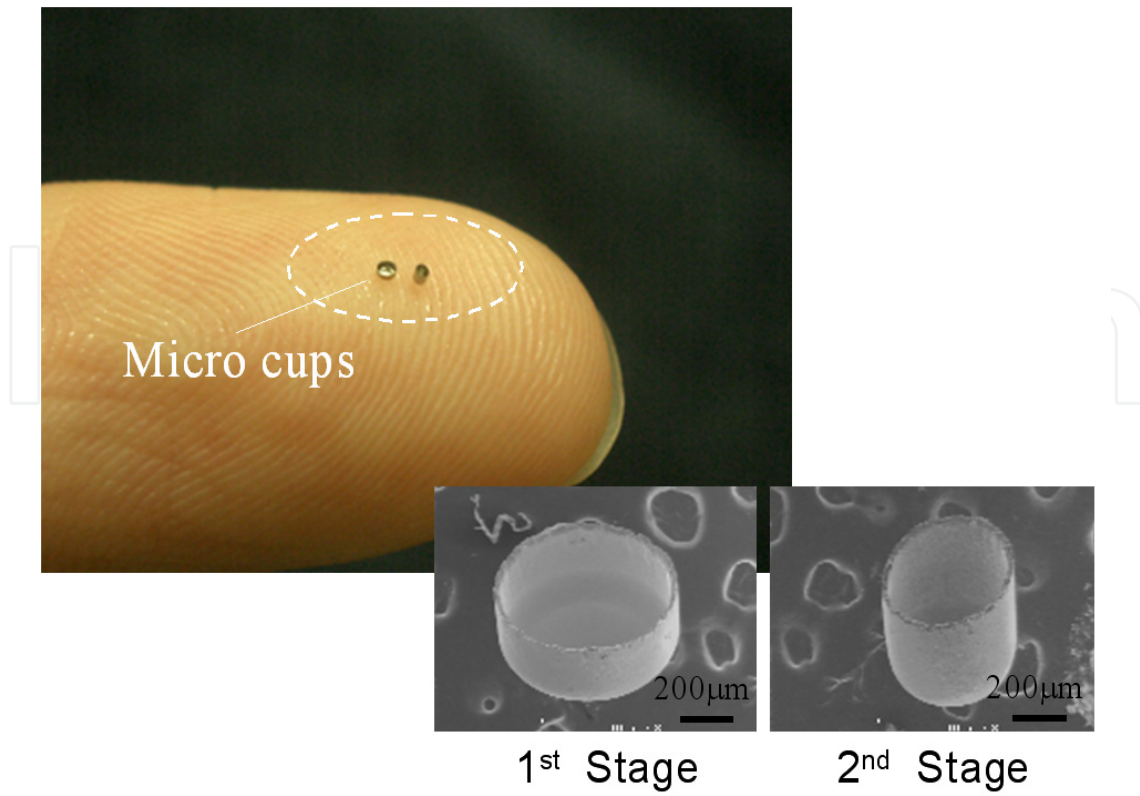


Figure 6. Appearance of drawn microcups on a forefinger and its SEM image

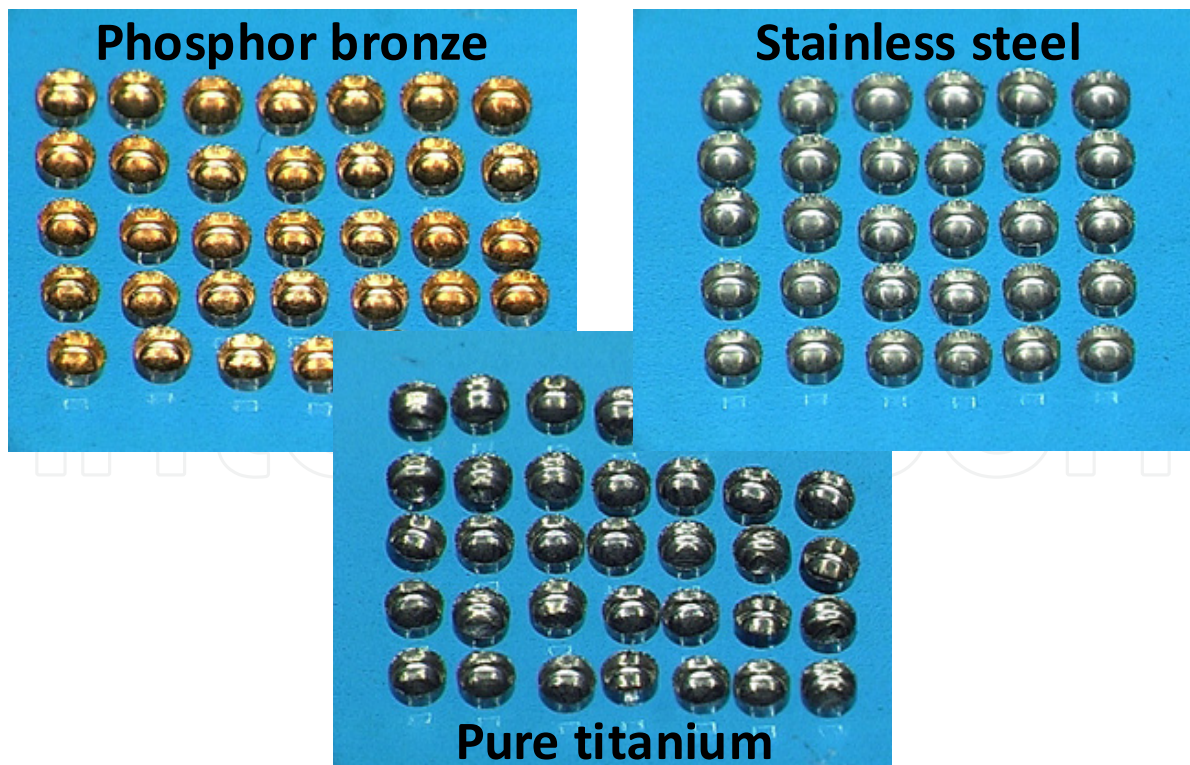


Figure 7. Appearance of drawn microcups with good reproducibility in three different materials, phosphor bronze, stainless steel, and pure titanium

3. FE analysis of surface roughness model

In order to analyse the influence of the surface asperities in wider range of roughness conditions of the tools and the materials, finite element (FE) analysis of the micro-deep drawing are carried out. To model from the microscopic roughness asperities to macroscopic material deformation behaviour, an advanced model with surface roughness is proposed.

3.1. Surface roughness model

A cyclic triangular concavo-convex configuration is applied to the FE model of micro-deep drawing. Fig.8 shows a schematic view of the surface roughness model. The blank diameter is 1.1mm and 0.02mm in thickness. The axisymmetric FE mesh sizes of quadrilateral four-node elements are $1\mu\text{m}\times 0.5\mu\text{m}$. A cyclic surface geometry is modelled as the height of the profile, R_z , and the pitch, P , both of which are variables. This surface model is constructed on whole surface elements of blank and tools. Some of the virtues to consider the surface asperity in the FE model are as follows (Shimizu et al., 2009):

1. It is possible to input the geometry of surface asperity as a parameter of the process.
2. It is possible to represent the local deformation of surface asperity caused by contact between the tool and the material.
3. It is possible to investigate the effect of local contact behaviour on global deformation properties, such as formability and forming accuracy.

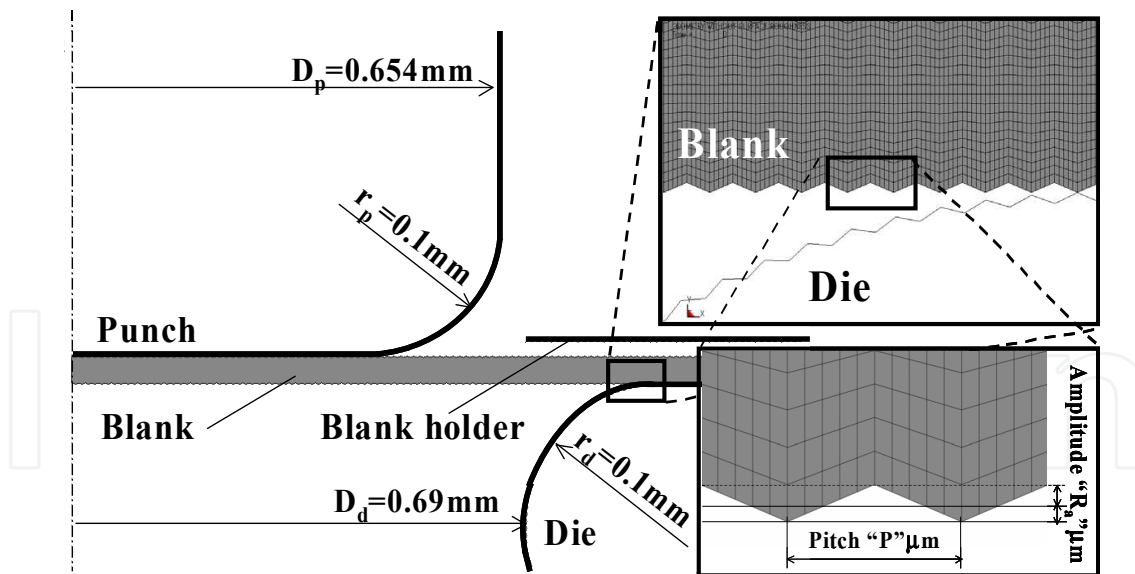


Figure 8. Schematic illustration of the surface roughness model and tool geometry

Fig.9 shows the distribution of equivalent plastic strain during the process with a surface roughness model (Shimizu et al., 2009). As shown in Fig. 9, plastic strain is observed at each local surface asperity. Particularly at a part of the sliding on the die corner and that of ironing, the amount of plastic strain of blank surface asperities is significant, due to the severe contact with the tool surface asperities.

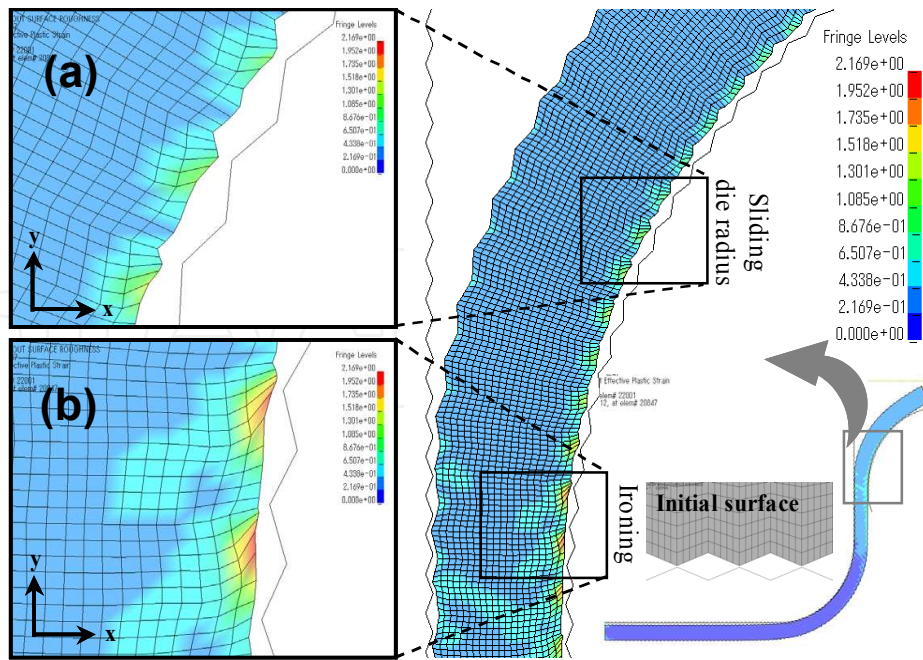


Figure 9. Distribution of equivalent plastic strain and close up images on part of (a) sliding with die corner and (b) ironing

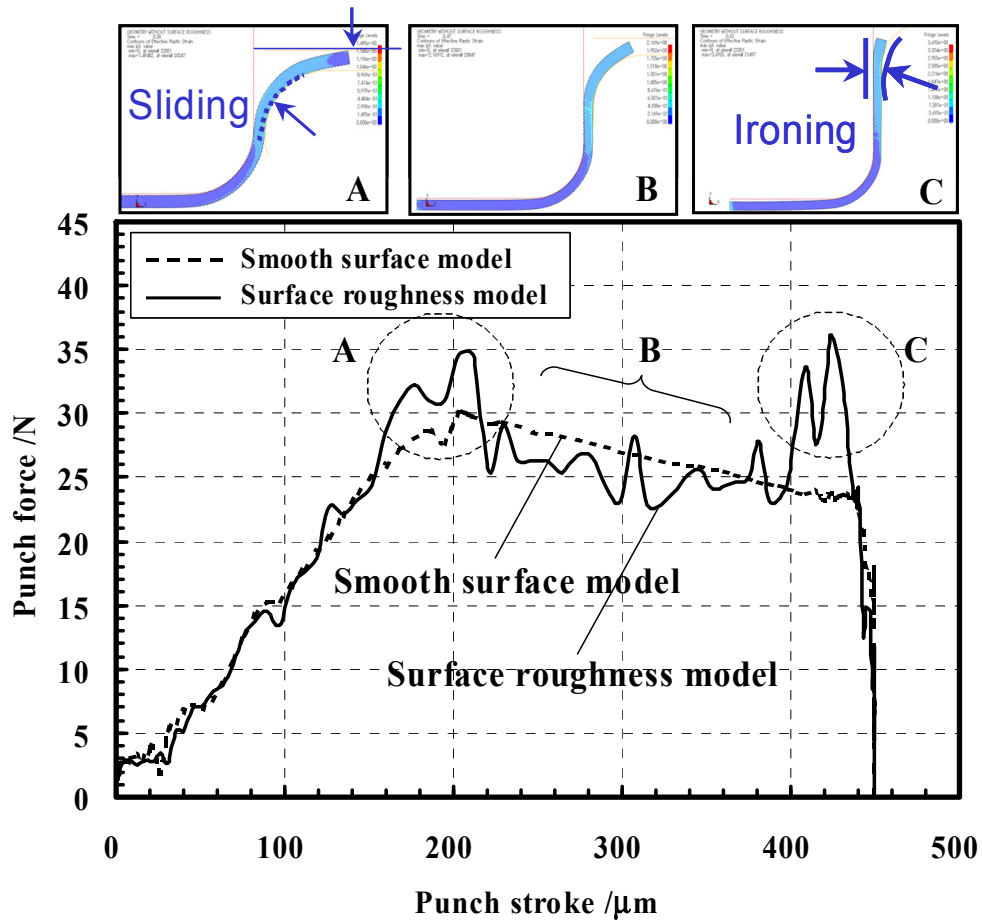


Figure 10. Comparison between punch force-stroke curves of “surface roughness model” and conventional “smooth surface model”

By comparing the surface roughness model with the smooth surface model, which is the conventional FE model with no roughness asperities, the difference with the surface roughness model can be recognized. As shown in Fig. 10, two peaks of maximum punch force are observed for the surface roughness model, while these peaks could not be observed in the smooth surface model. The first peak is under the sliding with a die corner (A) and the second peak is due to the ironing (C). Hence, by considering the local surface asperity on the model, effect of friction resistance of each surface asperity on global forming force are demonstrated.

3.2. Validation of surface roughness model

To validate the surface roughness model, the results of FE analysis are compared with the experimental results. As a representative evaluation, the micro-drawn cups of stainless steel (Fig.6) are precisely evaluated. As an evaluate item to investigate the deformation behaviour during forming process, thickness strain distribution of the drawn cup is precisely evaluated by digital image processing. Additionally, surface roughness of the drawn cups is also measured by confocal laser scanning microscope (LEXT OLS-3000, Olympus Co.).

The simulation is carried out with an explicit dynamic finite element code, LS-DYNA ver.970. Tools and blank dimensions are the same as those in the experiment (Fig.5). The blank model is assumed as isotropic elastoplastic body and it is modeled as an n^{th} power hardening law material ($\sigma=F\cdot\varepsilon^n$; σ : flow stress, F : strength coefficient, ε : true strain, n : n value). Tools such as a punch, a die and a blank holder are assumed as rigid bodies. All models are considered axisymmetric. Table 1 shows the mechanical properties of the blank and tools used in the simulation. The static and kinetic friction coefficients between the blank and the tools are assumed to be 0.05 and 0.03, respectively.

	Blank	Tool
Mass density ($\text{g}\cdot\mu\text{m}^{-3}$)	8.00×10^{-11}	8.00×10^{-7}
Young's modulus (GPa)	177	206
Poisson's ratio	0.3	0.3
F -value (GPa)	1.55	-
n -value	0.14	-

Table 1. Mechanical properties used in FE simulation

Fig.11 shows the comparison data of thickness strain distribution of both experiment and FE analysis (Manabe et al., 2008). General tendency of thickness variations in deep drawing process, such as the reduction at cup corner radius and the increase at cup edge, can be observed. Hence, the validation from the point of geometry and dimension of the model is demonstrated.

Fig.12 shows the comparison data of the surface roughness measured at defined 6 point of redrawn micro cups (Manabe et al., 2008). Although almost whole values are corresponded

to the result of FE analysis, only the difference at the inner surface is remarkable. From the observation of inner surface roughness of drawn cup, the surface roughening phenomenon seems to largely affect the surface quality of micro drawn cup. Therefore, in order to evaluate the surface quality more precisely, the consideration of the roughening phenomenon would be required.

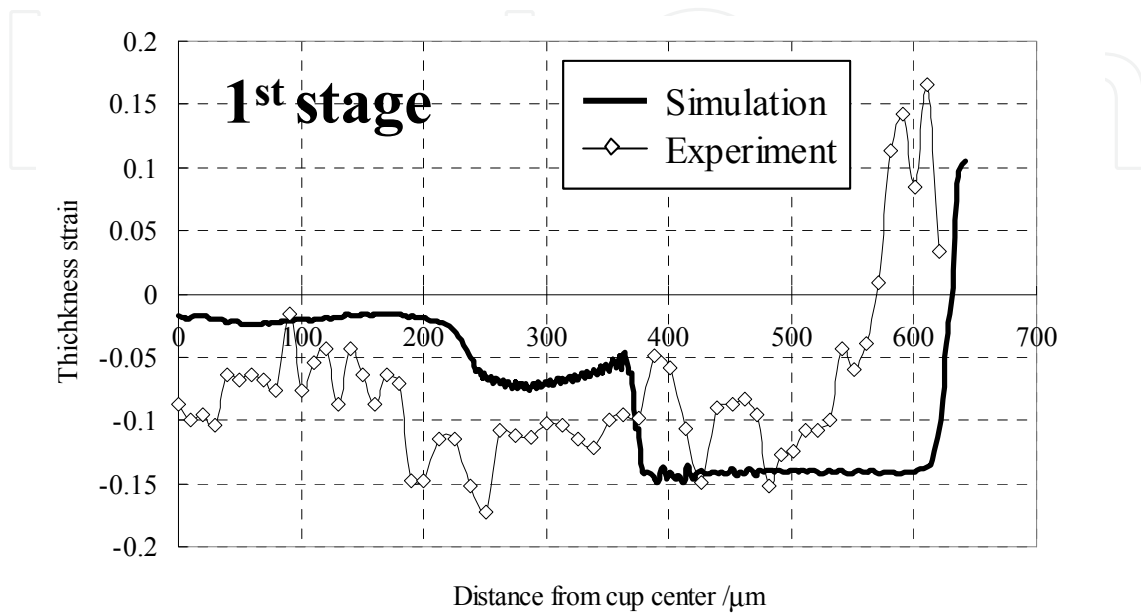


Figure 11. Comparison data of thickness strain distributions of micro-drawn cup

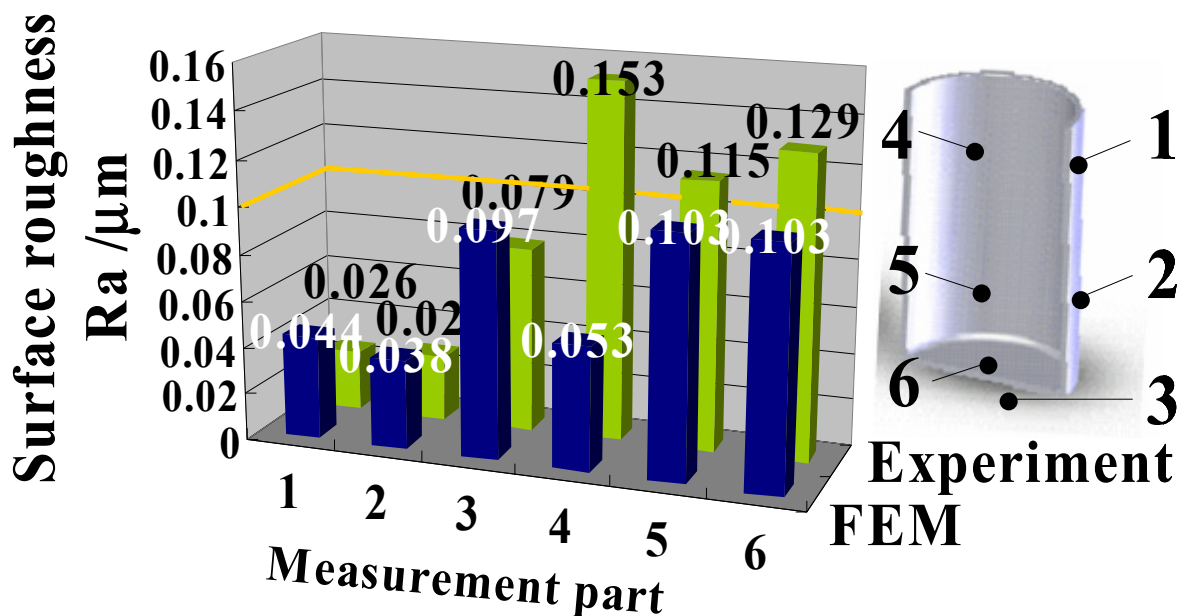


Figure 12. Comparison of surface roughness on each part of micro-drawn cup

Thus, by comparison of the experimental and FE simulation results for micro-deep drawing, the validation of surface roughness model are qualitatively demonstrated for the study on the effect of surface roughness for micro-deep drawing (Manabe et al. 2008).

4. Effect of surface topography on micro-deep drawability

By using the developed micro-deep drawing experimental set-up and proposed surface roughness model, the effect of the surface topography of tools and materials are experimentally and numerically investigated. The impact and sensitivity of the difference in surface properties during micro-scaled forming is demonstrated.

4.1. Effect of tool surface properties

Firstly, the effect of the tool surface properties is experimentally investigated. In order to study the sensitivity of tool surface properties on microformability, micro-deep drawing test is carried out with three different tools with the different surface properties. By comparing the forming results of the forming force and the surface quality of the micro-drawn cups, the effect of tool surface properties are discussed.

4.1.1. Materials and experimental conditions

The material used was stainless steel ultra-thin foils (JIS: SUS304-H, 20 μ m in thickness). Table 2 shows the mechanical properties of the used stainless steel ultra-thin foils, which was obtained by the tensile test.

Young's modulus	Yield stress	Tensile strength	Elongation
193[GPa]	1192[MPa]	1460[MPa]	1.5[%]

Table 2. Mechanical properties of stainless steel foils (JIS: SUS304-H, 20 μ m in thickness) used in the experiment.

As for the micro tools for the test, the same tools as mentioned in section 2.2 were used. In order to simplify the process, only the first stage process was compared between different surface conditions. To fabricate the microtools of different surface properties, air-blasting treatment and ion beam irradiation treatment were conducted for both micro-drawing die and punch. For the air-blasting treatment, glass powder of 53-63 μ m size was irradiated for 5-10min on the microtool surface to produce the rough surface. An air-blasting apparatus PNEUMA BLASTER SGK-DT (FUJI Manufacturing Co.) was used for the treatment. The ion-irradiation was performed by electron cyclotron ion shower system, EIS-200ER (ELIONIX Inc.), on the condition as shown in Table 3. Fig.13 shows the 3D surface images and the surface profile data of untreated, air-blasted and ion-irradiated micro-drawing punch obtained by laser scanning confocal microscope (LEXT OLS-3000, Olympus Co.).

Ion gas	Acceleration Voltage	Vacuum	Ion current density	Irradiation time	Irradiation angle
Ar	800eV	1x10 ⁻⁴ Pa	1.2mA/cm ²	5-10min	45°

Table 3. Conditions for ion beam irradiation

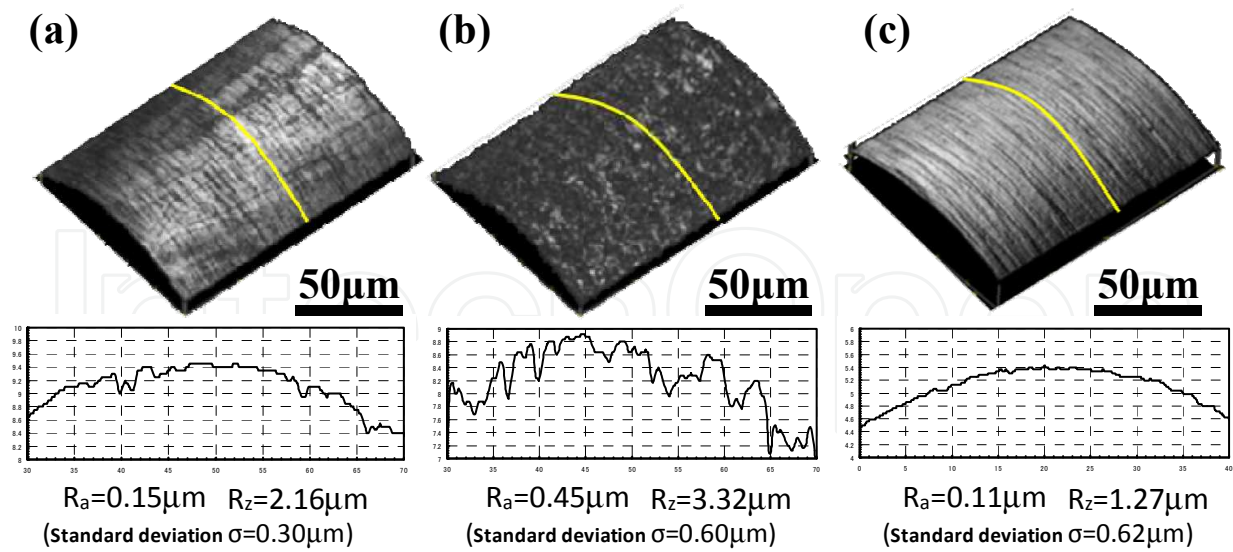


Figure 13. 3D surface images of the micro drawing punch with different surface characteristics, (a) Untreated tool (b) Air-blasted tool (c) Ion-irradiated tool

For the untreated tools, machined traces on the circumferential direction of punch surface are observed. While, for the air-blasted tools, the maximum height of the surface roughness is remarkably rough and the dispersion of the maximum height roughness is also large. In contrast, for the ion-irradiated tools, though machining marks can slightly be observed, peak of the asperities are removed by ion sputtering and smooth surface with no directional property can be obtained.

The tests were conducted under a nonlubricated condition. The drawing speed was 0.4mm/s and no blank holder force (BHF) was applied as mentioned. To evaluate the formability under each surface condition, punch force was measured with a micro-load cell. Additionally, to evaluate the drawn microcups, the cup surface roughness was measured by laser scanning confocal microscope (LEXT OLS-3000, Olympus Co.).

4.1.2. Punch load-stroke curves

In order to compare the punch force-stroke curve in each condition, the punch force is normalized. Normalized punch force, \bar{P} , during the deep drawing process can be described as

$$\bar{P} = P / (\pi \cdot d_p \cdot t_0 \cdot \tau_y) \quad (1)$$

,where, d_p is punch diameter, t_0 is initial foil thickness, and τ_y is shear yield stress of the blank material (Hu et al., 2007). The punch stroke is normalized with the drawing punch diameter, d_p . In this normalization, higher normalized force indicates the higher fraction of friction force to the whole forming force during the process. Fig.14 shows the comparative data of normalized punch load-stroke curves between the three tools of different surface asperities. The error bar of the curves indicates the standard deviation of the normalized punch force. Fig 15 summarizes the standard deviations of the maximum drawing and ironing force in each load-stroke curve.

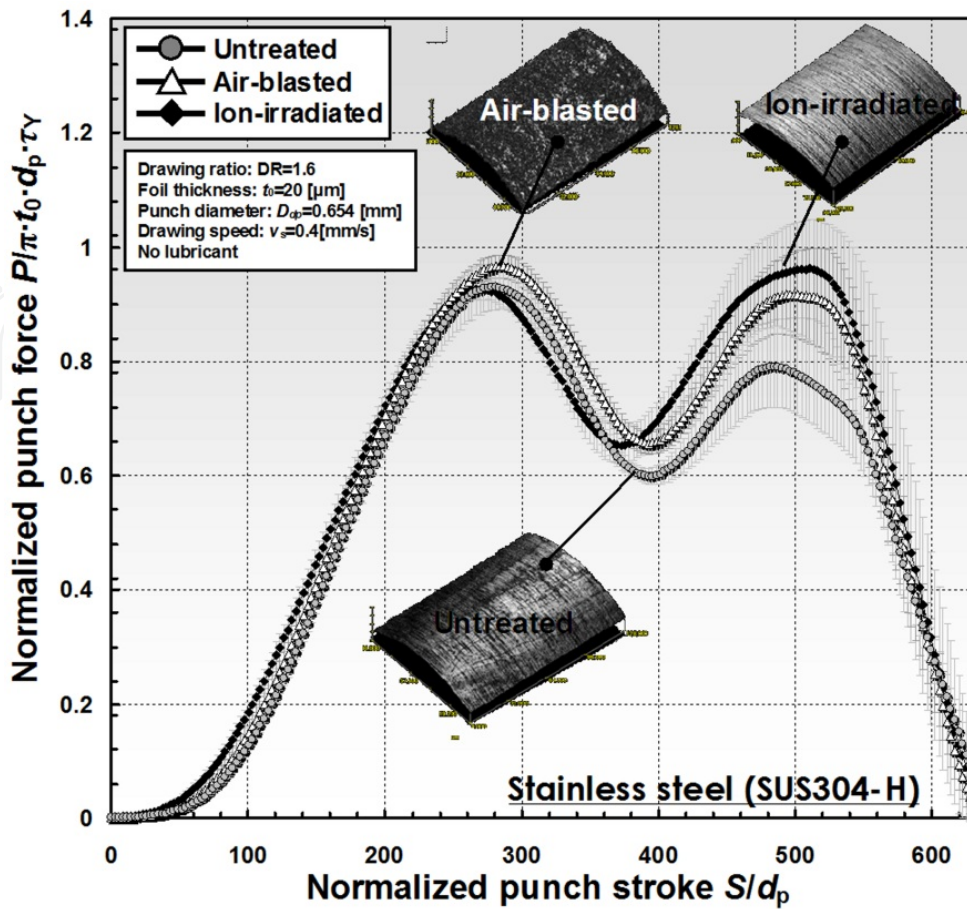


Figure 14. Comparison of normalized punch force-stroke curves between 3 tools with different surface properties

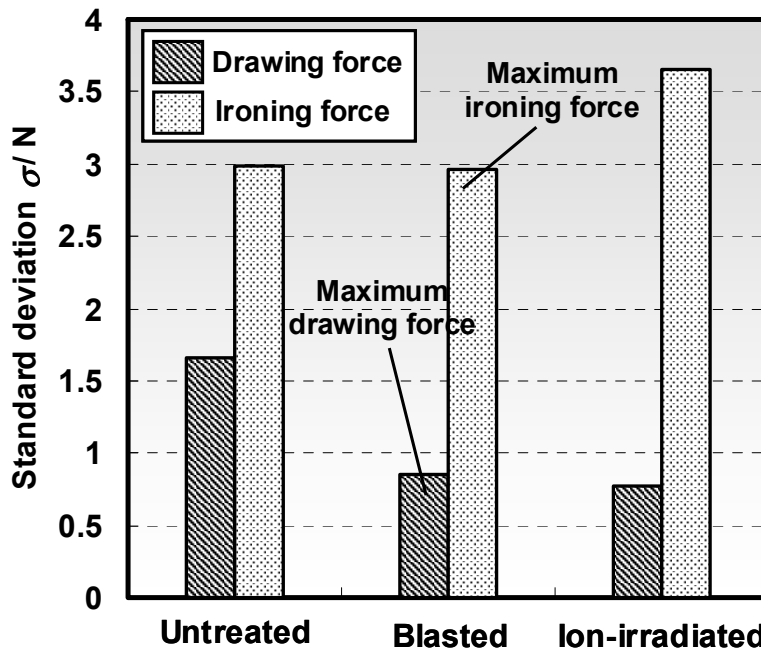


Figure 15. Comparison of standard deviation of maximum drawing and ironing force in each tool surface condition

The air-blasted tool shows the maximum drawing force, while the maximum ironing force is indicated by the ion irradiated tools. In addition, the both the lowest drawing and ironing force are shown by the untreated tool. In comparison of the dispersion of the force in each tool condition, the widest variation in maximum drawing force is observed for the untreated tool and the larger dispersion in maximum ironing force is indicated by the ion-irradiated tool. The wider variation of the ironing force data for every tool conditions seems to be attributed to the high contact pressure induced by the ironing process. Thus, the difference in the effect of tool surface properties on friction is markedly observed.

4.1.3. Surface quality of drawn cups

Fig.16 shows the surface images of the upper and the lower sides of the microcup wall of outer surface (Shimizu et al., 2009). The surface of the microcup has a large difference, as shown in the figure. In particular, for the microcup drawn by the ion-irradiated tool, scratches and chippings of the material caused by the adhesion are remarkable. In contrast, although the tool surface has the roughest surface for the air-blasted tool, the surface of the microcup is smoothed by sliding with the die, and better surface quality is observed. Furthermore, a roughened surface similar to an orange peel surface is observed at the lower part of the microcup drawn by the untreated tool. While, sliding traces with the die are observed under the conditions with the air-blasted and ion-irradiated tool.

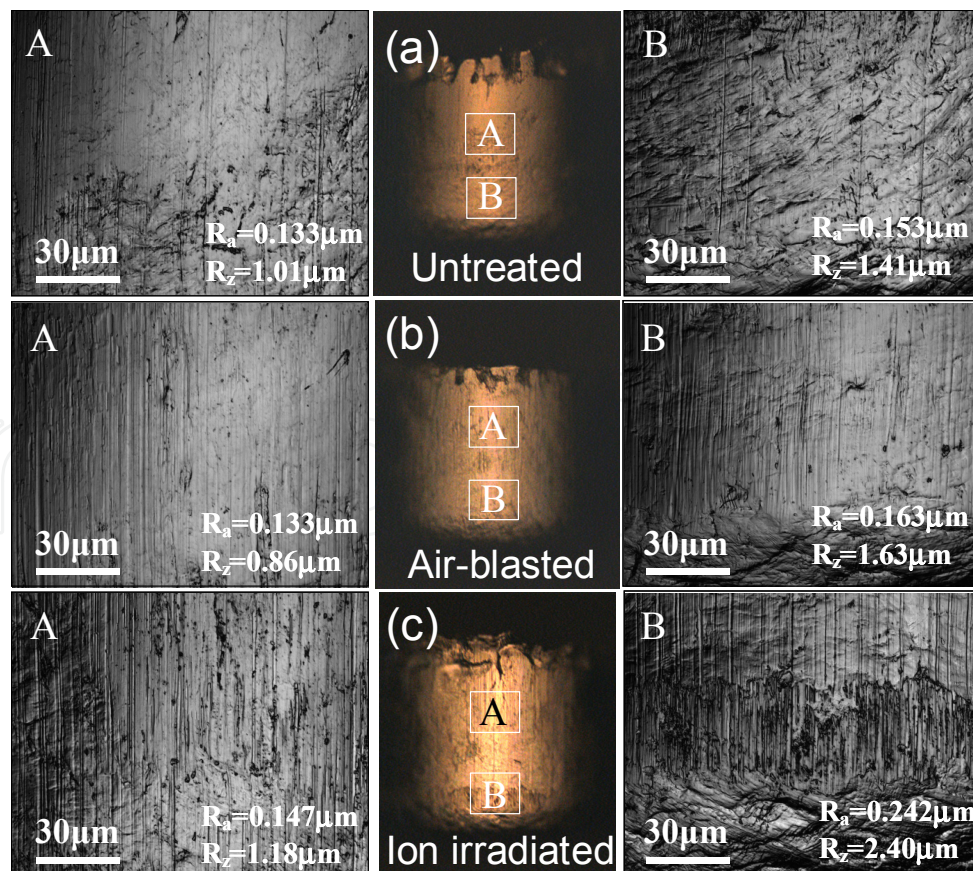


Figure 16. Surface images of microcup wall using 3 tools with different surface properties

The higher value and wider dispersion of the ironing force under the ion-irradiated tool appears to be due to the strong plowing of the wear particles. In fact, Yang et al. reported that WC particles would be exposed by the ion irradiation of WC-Co hard alloy, due to the difference in sputtering rate between the WC and Co (Yang et al., 2008). Since Co particles are removed from the surface, the WC particles lose the binding agents and are easily to drop off from the surface. Therefore the dropped WC particles seem to scratch and plough the surface of work material. Thus, remarkable difference in interfacial behaviour between the tool and material are experimentally demonstrated.

4.2. Effect of material surface properties

Secondly, the effect of material surface properties is studied. In order to compare the influence of material surface properties on micro-deep drawability, we focused on the aluminium foils, which have the two different surfaces in one foil sheet due to the manufacturing process of 2 layers rolling.

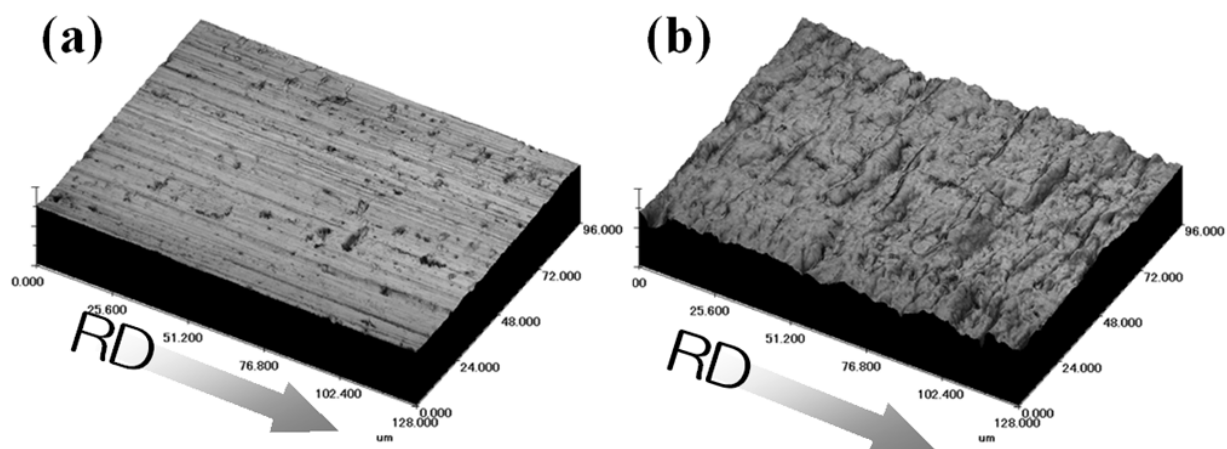


Figure 17. Surface images of 1N30 pure aluminum foil (a) bright surface, (b) mat surface

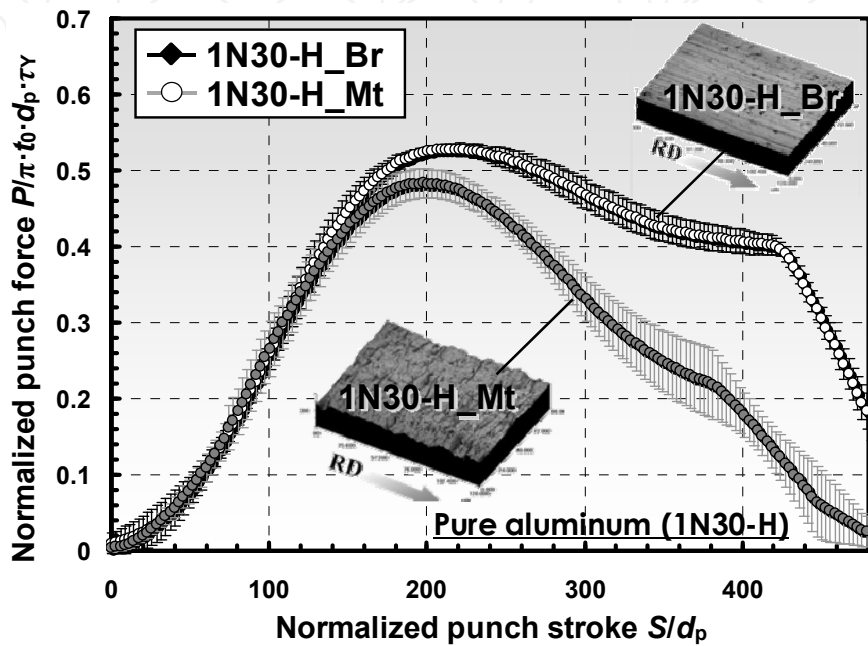
4.2.1. Materials and experimental conditions

As the aluminium foil, pure aluminium (JIS: 1N30) was used as test specimen. Two kinds of pure aluminium of spring-hard material (JIS:1N30-H) and annealed material (JIS: 1N30-O) were investigated. The nominal initial thickness of the both foils were $20\mu\text{m}$. Table 3 shows the mechanical properties of the 1N30-H and the 1N30-O pure aluminium foil, which was provided by the supplier.

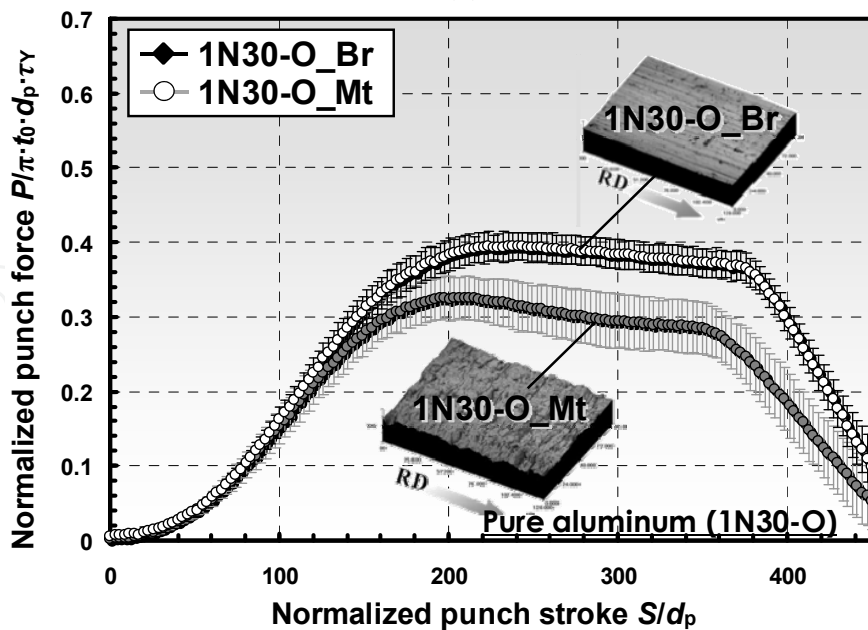
Fig.17 shows the surface images of the 1N30-H pure aluminium. The bright surface has smooth roughness of $1.02\mu\text{mRz}$, while the mat surface has rough surface with $1.64\mu\text{mRz}$. The contact between the bright surface and the die surface is defined as contact condition Br, and the condition for mat surface is defined as condition Mt.

Material	Young's modulus	Yield stress	Tensile strength	Elongation
1N30-H	70[GPa]	159[MPa]	177[MPa]	2.7[%]
1N30-O	70[GPa]	69[MPa]	88[MPa]	22.0[%]

Table 4. Mechanical properties of pure aluminium foils (JIS: 1N30, 20 μ m in thickness) used in the experiment.



(a)



(b)

Figure 18. Punch force-stroke curves for comparing different material surface conditions (a) 1N30-H, (b) 1N30-O

The tests were carried out under the same conditions as previous section. Similarly, punch load during the process and surface quality of the cup after drawing were evaluated.

4.2.2. Punch load-stroke curves

Fig. 18 shows the normalized punch-stroke curves, which compares between different surface conditions of 2 kinds of pure aluminium foils, 1N30-H, and -O.

For both materials, the condition Br indicates the higher drawing and ironing force. Although the difference of maximum drawing force is almost no difference between condition Br and Mt for both 1N30-H and 1N30-O aluminium foil, maximum ironing force for the 1N30-H indicates larger difference than that of 1N30-O, as shown in Fig 18(a). In order to investigate the cause of these tendencies of each difference, the surface state of the drawn microcup is observed in following section.

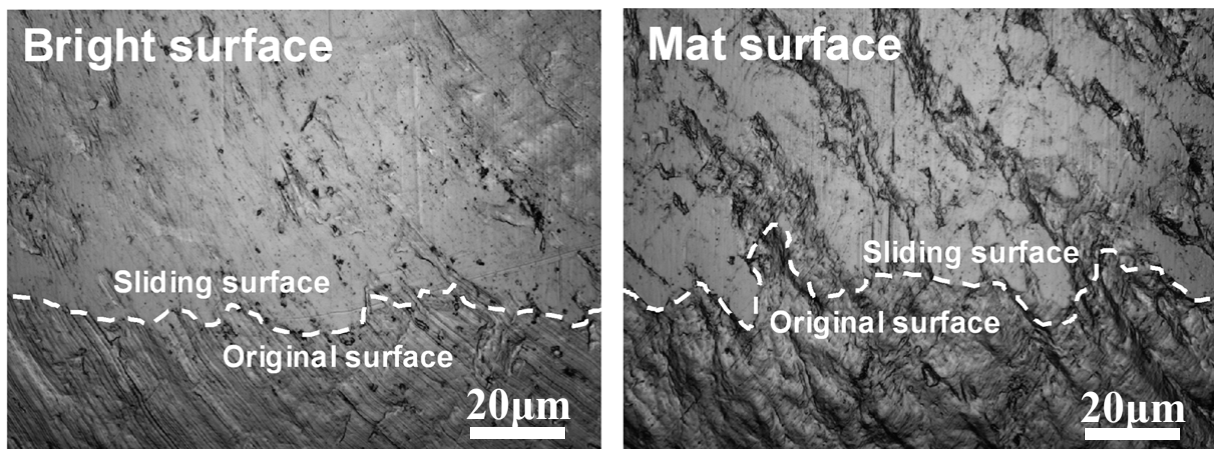


Figure 19. Surface images at bottom area of micro-drawn cup wall

4.2.3. Surface quality of drawn cups

Fig.19 compares the surface images of the bottom area of drawn cup wall surface under 2 contact conditions. As shown in the figure, the boundary of the sliding surface and the original surface with rolling traces can be clearly recognized. In comparison of the sliding surfaces, although almost of the whole area of the cup wall is smoothed with die surface for the bright surface condition, mat surface condition has the area, which does not contact

with the die surface. This suggests that the real area of contact is less in condition Mt than that in condition Br during the ironing, and it would be responsible for the lower friction resistance during the forming. Therefore, it is clear that the initial material surface roughness is also responsible for the friction resistance during sheet metal forming.

4.3. FE analysis with surface roughness model

In order to discuss the obtained experimental results in detail, and to evaluate the experimental results more generally, FE analysis with proposed surface roughness model is carried out.

4.3.1. Simulation conditions

The simulation was carried out with the condition as mentioned in section 3.2. To study the effect of combination of surface geometry between the blank and the tools on formability, different combinations of surface geometries were analyzed. The combination conditions of the process are given in Table 5. To compare and quantify the effect of the surface topographical interaction between the tool and the material, the punch forces during the process were calculated.

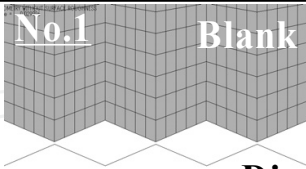
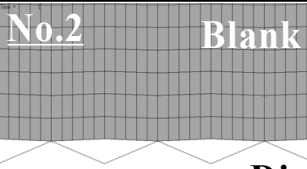
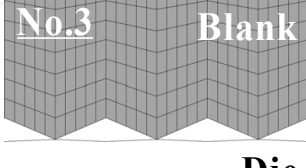
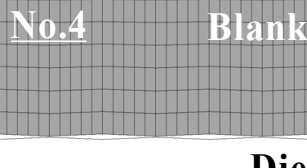
		Blank surface geometry	
		$Rz=0.5\mu\text{m}$, $P=5\mu\text{m}$	$Rz=0.05\mu\text{m}$, $P=5\mu\text{m}$
Tool surface geometry	$Rz=0.5\mu\text{m}$ $P=5\mu\text{m}$	No.1 Blank  Die	No.2 Blank  Die
	$Rz=0.05\mu\text{m}$ $P=5\mu\text{m}$	No.3 Blank  Die	No.4 Blank  Die

Table 5. Combination conditions of surface geometry between blank and tools

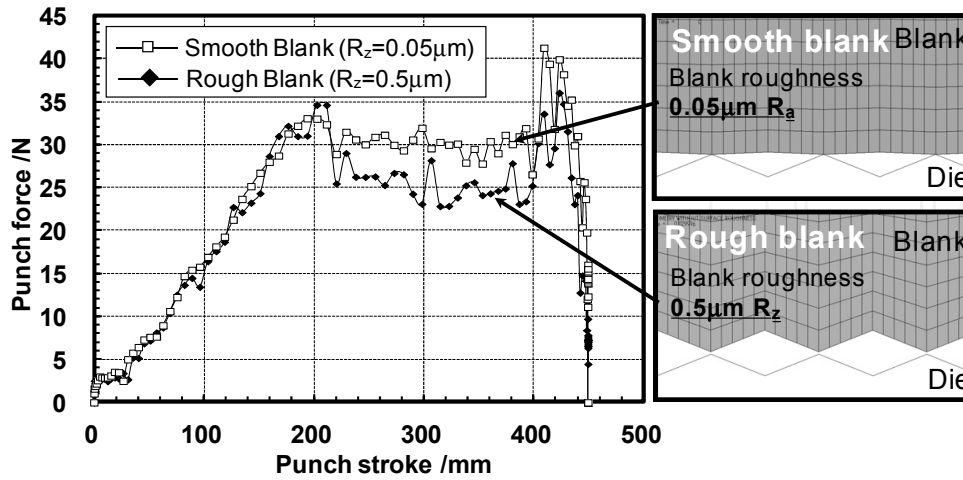
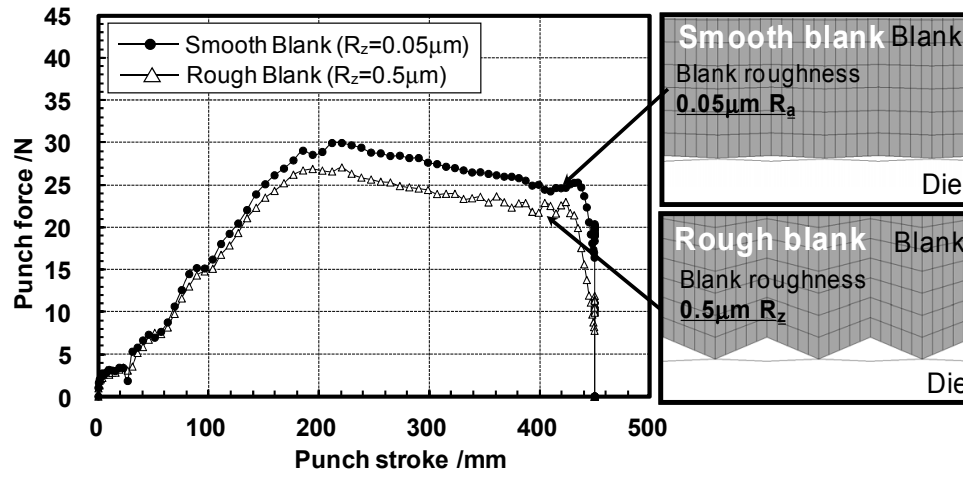
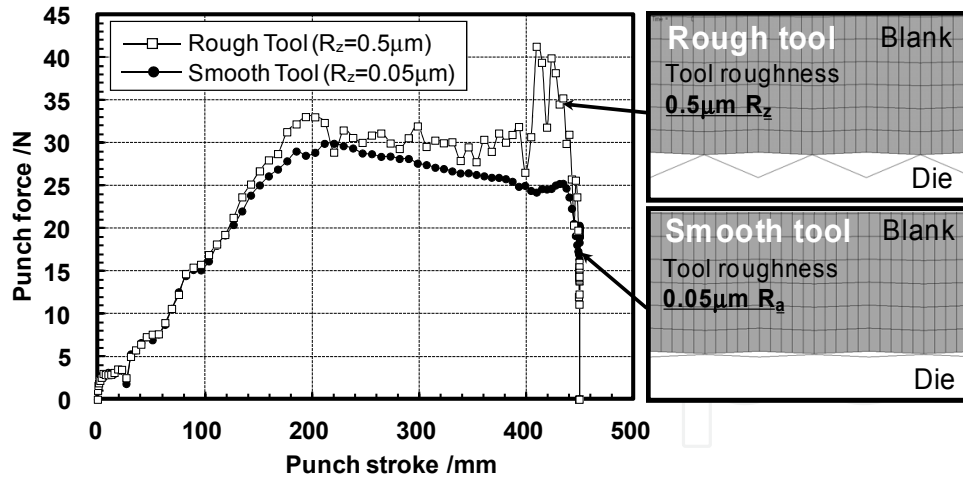


Figure 20. FEM results of load-stroke curve under different surface conditions between tool and material (a) Effect of tool surface amplitude (b) Effect of blank surface amplitude with smooth tool, (c) Effect of blank surface amplitude with rough tool

4.3.2. Simulation results

Fig.20 (a) shows the effect of roughness amplitude of a tool with same smooth material surface on formability (Condition No.2 and 4) (Shimizu et al., 2009). The curve obtained for the rough tool indicates the higher punch forces than those of the smooth tool. The difference in ironing force is particularly large. This tendency was also observed in the experimental results of the comparison between the untreated tool (smooth) and the air-blasted tool (rough), as shown in Fig. 14. From the deformation history in the analysis, it can be seen that, if the tool surface asperity are sharper than the blank surface asperity, the plastic deformation of the blank surface asperity would be easily occurred, due to the intensive surface pressure. In the actual contact behavior during the process, this phenomenon in FE analysis could be translated to the fracture of oxide film layer due to the high normal pressure. It would easily induce the adhesion or the plowing and increases the friction.

Fig. 20 (b) and (c) show the effect of blank roughness amplitude under the same tool surface condition (Shimizu et al., 2009). As for the condition with the smooth amplitude tool (Condition No.3 and 4) as shown in Fig. 20 (b), the punch force of the rough material is lower than that of the smooth material. The similar tendency in the experiment is already shown in Fig. 18(a) and (b). As mentioned from the observed surface images of micro-drawn cup in Fig.19, since the real area of contact under the smoother amplitude blank is much larger than that of rough amplitude blank, the friction force will increase and it results in the higher forming force.

While for the condition with a rough amplitude tool (Condition No.1 and 2) shown in Fig.20 (c), the maximum drawing and ironing force indicates almost the same value between the conditions. This shows the higher impact of the tool surface roughness than the material surface roughness. Since the harder tool surface asperities would plow the softer material surface, the material surface roughness seems to be less influence on the friction resistance under the contact with the rough tool surface.

Thus, local interfacial behavior in micro-deep drawing could be explained on the basis of classic theory of conventional tribology. However, a feature of the micro-scale region appears to be the higher sensitivity of the global forming behavior to the microscopic surface properties. Therefore, the proper surface design of tools and work materials in micro-scale becomes significantly more important than in conventional macro-scale.

5. Conclusion

From the perspective of the significant importance of tribological behaviour under dry friction in micro-sheet metal forming, this chapter has created an overview of the effect of surface topography of tools and workpieces on micro-sheet formability.

The advanced development of the micro-deep drawing experimental system has realized the investigation under the actual micro-scale range forming behaviour, such as the

fabrication of tiny micro cups with minimum 0.5 mm in diameter. By providing the different microtools with different surface properties, the high sensitivity of the forming force to the different surface conditions of micro tools has been clearly recognized. Especially, the ironing force and its deviation have the large differences. The surface observation of the drawn cup demonstrates the importance of the tool surface roughness and the material compatibility between the tool and material, in view of the occurrence of adhesion and abrasive wear. In the additional investigation of the influence of material surface roughness, the higher friction force for the bright smooth surface is indicated. This appears to be attributed to the real area of contact during the process, which is strongly dependent on the initial surface geometry of the work material.

Furthermore, the FE model with surface asperities has been proposed and the availability and the validation of this model are demonstrated. The calculation results of this surface roughness model under the different combination conditions of surface asperities are well corresponded to the experimental results. The general tendency of the interaction of the surface asperities between the tools and the workpieces is explainable in terms of the classic theory of tribology.

Since the sensitivity to the surface properties for the global forming behaviour becomes higher with decreasing the scale dimensions, the proper design of the tool and the material are required more precisely in microforming. In other words, the microscopic geometry of the surface of tools and materials would become a significant parameter of controlling global deformation behaviour in microforming. The tribological optimisation by the surface texturing technology for micro-tooling and materials would be the future tasks.

Author details

Tetsuhide Shimizu, Ming Yang and Ken-ichi Manabe
Tokyo Metropolitan University, Japan

Acknowledgement

The authors gratefully acknowledge the support from JSPS (Japan Society for the Promotion of Science) under a JSPS Research Fellowships for Young Scientists. In the whole experimental work of micro-deep drawing, the authors also particularly indebted to Mr. Kuniyoshi Ito at Micro Fabrication Laboratory (formerly at Seki Corporation) for his valuable advice and support.

6. References

Aizawa, T., Itoh, K., Iwamura, E. (2010). Nano-laminated DLC Coating for Micro-Stamping, *Proceedings of the International Conference on Metal Forming, Steel Research International*, vol.81-9, (2010), pp.1169-1172, Toyohashi, Japan, September 19-22, 2010

- Bhushan, B. (2002). *Introduction to Tribology*, Wiley, New York
- Engel, U. (2006). Tribology in Microforming, *Wear*, Vol.260, (2006), pp. 265-273
- Fuentes, G.G., Diaz de Cerio, M.J., Rodriguez, R., Avelar-Batista, J.C., Spain, E., Housden, J., Qin, Y. (2006). Investigation on the Sliding of Aluminium Thin Foils against PVD-coated Carbide Forming Tools during Micro-forming, *Journal of Materials Processing Technology*, vol.177, (2006), pp.644-648
- Fujimoto, K., Yang, M., Hotta, M., Koyama, H., Nakano, S., Morikawa, K., Cairney, J.(2007). Fabrication of Dies in Micro-scale for Micro-sheet Metal Forming, *Journal of Materials Processing Technology*, vol.177, (2006), pp.639-643
- Geiger, M.; Kleiner, M. ; Eckstein, R. ; Tiesler, N.& Engel, U. (2001). Microforming, *Annals of the CIRP - Manufacturing Technology*, Vol.50, Issue 2, (2001), pp. 445-462
- Hanada, K., Zhang, L., Mayuzumi, M., Sano, T. (2003). Fabrication of Diamond Dies for Microforming, *Diamond and Related Materials*, vol.12, (2003), pp.757-761
- Hu, Z. & Vollertsen, F. (2007); Tribological Size Effect in Sheet Metal Forming, *Proceedings of the International Conference on Tribology in Manufacturing Process, ICTMP2007*, pp.163-168, Yokohama, Japan, September 24-26, 2007
- Krishnan, N., Cao, J., Dohda, K. (2007). Study of the Size Effect on Friction Conditions in Micro-Extrusion. Part 1. Micro-Extrusion Experiments and Analysis, *ASME Journal of Manufacturing Science and Engineering*, vol.129 No.4, (2007), pp.669-676
- Manabe, K., Shimizu, T., Koyama, H., Yang, M., Ito, K. (2008). Validation of FE simulation based on surface roughness model in micro-deep drawing, *Journal of Materials Processing Technology*, vol. 204, (2008), pp.89-93
- Mori, L., Krishnan, N., Cao, J., Espinosa, H. (2007). Study of the Size Effects and Friction Conditions in Micro-Extrusion. Part II. Size Effect in Dynamic Friction for Brass-Steel Pairs, *ASME Journal of Manufacturing Science and Engineering*, vol.129 No.4, (2007), pp.677-689
- Putten, K.V., Franzke, M., Hirt, G. (2007). Size effect on friction and yielding in wire flat rolling, *Proceedings of the 2nd International Conference on New Forming Technology, ICNFT 2007*, pp. 583-592, Bremen, Germany, September 20-21, 2007
- Shimizu, T., Murashige, Y., Ito, K., Manabe, K. (2009). Influence of surface topographical interaction between tool and material in micro-deep drawing, *Journal of Solid Mechanics and Materials Engineering*, Vol.3 No.2, (2009), pp.397-408
- Vollertsen, F., Biermann, D., Hansen, H.N., Jawahir, I.S. & Kuzman, K. (2009). Size Effect in Manufacturing of Metallic Components, *Annals of the CIRP - Manufacturing Technology*, Vol.58, (2009), pp. 566-587
- Vollertsen, F.& Hu, Z. (2006). Tribological Size Effects in Sheet Metal Forming Measured by a Strip Drawing Test, *Annals of the CIRP - Manufacturing Technology*, Vol.55, Issue 1, pp. 291-294
- Vollertsen, F.& Hu, Z. (2008). Determination of Size-Dependent Friction Functions in Sheet Metal Forming with Respect to the Distribution of the Contact Pressure, *Production Engineering*, vol.2-4, (2008), pp.345-350

Yang, M. & Osako, A.(2008). Application of Ion Irradiation for Surface Finish of Micro-forming Die, *Journal of Materials Processing Technology*, vol. 201, (2008), pp.315-318

IntechOpen

IntechOpen